A Controllable Thyristor-Based Commutation Failure Inhibitor for LCC-HVDC Transmission Systems

Sohrab Mirsaeidi, *Member, IEEE*, Dimitrios Tzelepis, *Member, IEEE*, Jinghan He, *Fellow, IEEE*, Xinzhou Dong, *Fellow, IEEE*, Dalila Mat Said, *Senior Member, IEEE*, and Campbell Booth

***Abstract*—Commutation failure is a serious malfunction in line-commutated high voltage direct current (HVdc) converters which is mainly caused by the inverter ac faults, and results in a temporary interruption of transmitted power and damage to the converter equipment. In this article, a controllable commutation failure inhibitor (CCFI) is developed which obviates the main drawbacks of the existing power electronic based and fault current limiting based strategies. Under normal circumstances, the developed CCFI improves the steady-state stability and the power transfer capability of the inverter ac lines, while it does not cause excessive voltage stress on the converter valves. In addition, it would reduce the risk of commutation failure occurrence, since it does not lead to any voltage drop in the commutation circuit. When a fault occurs at one of the inverter ac systems, its corresponding CCFI limits the fault current depending on the reduced extinction angle. This would not only inhibit the successive commutation failures on the HVdc converter, but also extend the lifetime of components in the inverter ac systems. The practical feasibility of the developed CCFI is assessed through laboratory testing, using a real-time Opal-RT hardware prototyping platform. The obtained results indicate that the developed CCFI can reliably inhibit the commutation failures during various types of faults.**

***Index Terms*—Commutation failure, high voltage direct current (HVdc) transmission, hybrid ac/dc power grids, line-commutated converters.**

I. Introduction

LINE-COMMUTATED converter based HVdc (LCC-HVdc) technology has been extensively utilized around the world for long-distance bulk-power transmission due to its merits such as the thyristors superior power handling capability and lower operating power losses [1], [2]. Nevertheless, the development of LCC-HVdc systems suffers from some well-known challenges such as poor voltage regulation ability and vulnerability to commutation failures during inverter ac fault incidents, which can lead to a temporary cessation of transmitted power, overheating of the valves, and misoperation of the protective relays [3].

Commutation failures are frequent dynamic incidents which have been recorded in several existing LCC-HVdc projects around the world [4]. They would become more problematic when several HVdc links terminate in one ac system such as concurrent commutation failures and forced blocking of five converter stations resulting from an inverter ac fault in South China Power Grid in 2010. This accident led to a drastic frequency reduction in the inverter ac system and an overload of the adjacent HVac lines. Also, the generators at the rectifier side were tripped and spinning reserves were activated at the inverter side to compensate for the loss of active power transfer [5]. Accordingly, commutation failure elimination has been extensively studied over the decades and a large number of approaches have been proposed. These approaches can be classified into three main categories, i.e., modification of the HVdc control system, deployment of power electronic based methods, and fault current limiting based techniques.

For the approaches based on modification of the HVdc control system, it is pointed out by [6], [7] that the commutation failure cannot be entirely eliminated if the fault takes place very close to the inverter station. Therefore, the main targets of these approaches are to either reduce the probability of commutation failures or to expedite the HVdc system recovery after the commutation failure. The most commonly used method in this group is to immediately advance the applied firing angle to the converter thyristors after an inverter ac fault occurrence so that the commutation margin is enlarged. The main differences between the approaches of this group are:

1) the technique of detecting faults such as using symmetrical components [8] or power component fault detection method [9];
2) the method of determining the desired firing angle such as direct measurement of commutation margin using the waveforms of the anode–cathode valve voltages [8] or deployment of fuzzy logic based methods [10], [11];

Manuscript received February 14, 2020; revised July 1, 2020; accepted August 27, 2020. Date of publication September 2, 2020; date of current version November 20, 2020. This work was supported in part by the National Key Research and Development Plan of China under Grant 2018YFB0904602, in part by the Fundamental Research Funds for the Central Universities under Grant 2019RC051, and in part by the PHOENIX Project UK (SPTEN03). Recommended for publication by Associate Editor F. Wang. *(Corresponding author: Sohrab Mirsaeidi.)*

Sohrab Mirsaeidi and Jinghan He are with the School of Electrical Engineering, Beijing Jiaotong University, Beijing 100044, China (e-mail: msohrab@bjtu.edu.cn; jhhe@bjtu.edu.cn).

Dimitrios Tzelepis and Campbell Booth are with the Department of Electronic and Electrical Engineering, University of Strathclyde, G1 1XW Glasgow, U.K. (e-mail: dimitrios.tzelepis@strath.ac.uk; campbell.d.booth@strath.ac.uk).

Xinzhou Dong is with the Department of Electrical Engineering, Tsinghua University, Beijing 100084, China (e-mail: xzdong@mail.tsinghua.edu.cn).

Dalila Mat Said is with the Centre of Electrical Energy Systems, Faculty of Electrical Engineering, Universiti Teknologi Malaysia, Johor Bahru 81310, Malaysia (e-mail: dalila@utm.my).

This article has supplementary downloadable material available at https://ieeexplore.ieee.org, provided by the authors. Color versions of one or more of the figures in this article are available online at https://ieeexplore.ieee.org.

Digital Object Identifier 10.1109/TPEL.2020.3021284

3) the accuracy in calculation of firing angle advancement which results from considering/neglecting some of the commutation failure influencing factors including dc current [6], ac voltage, commutation inductance [8], [12], phase-angle shift, fault severity [13], and initial fault voltage angle [14];
4) the execution speed of firing angle advancer.

However, the effectiveness of such methods is highly dependent on the fault initiation time, because if the fault occurs at the beginning or during the commutation process, the commutation failure cannot be avoided. Moreover, it is identified in [15] that advancing the firing angle augments the consumed reactive power by the converter and will further increase the inverter ac bus voltage drop. As a result, considering a limit for the extinction angle enhancement in these approaches would be necessary. In [5], a dc predictive control algorithm is developed by modifying the rectifier control system, in which the dc current order is reduced after the detection of an ac voltage disturbance. However, concerning the long distance of the HVdc lines, changing the current order at the rectifier station may not be rapid enough to deal with the commutation failure. The authors in [16]–[20] propose a voltage-dependent current-order limit (VDCOL) strategy to safeguard the HVdc system against commutation failures by limiting the current order according to the ac voltage or dc voltage. However, the variation of dc current is not considered in these studies and there is some room for further improvement [21].

Among the power electronic based methods, the most well-known one is to employ capacitor-commutated converters (CCCs) with fixed capacitors between the thyristor valves and the converter transformer [22]. The capacitors contribute to enhance the magnitude of commutating voltages and provide a larger commutation margin so that the commutation failure is inhibited. In addition, they improve the power factor of the inverter ac system through the reduction of reactive power consumption. However, as identified by [23], the insertion of large commutation capacitors leads to the significant voltage stress on the valves (typically in the range of 2 to 3 p.u.) during the normal operation of the converter which shortens its lifetime. Moreover, there is a possibility of ferroresonance occurring in the circuit formed by the ac system, commutation capacitors, and converter transformer. In [22], an alternative configuration, referred to as controlled series capacitor converter (CSCC), is introduced where the series capacitors are inserted between the inverter ac bus and the inverter ac system. In the CSCC configuration, even though the capacitor values can be adjusted similar to the thyristor controlled series compensation (TCSC) schemes, the controllability of capacitors is only used for the prevention of ferroresonance challenge.

The aim of the proposed methods in the third category is to prevent the commutation failure through ac voltage drop compensation by suppressing the fault current magnitude. The most popular method in this group is to use superconducting fault current limiters (SFCLs). In [24], the effectiveness of SFCL on commutation failure mitigation is qualitatively studied, while authors of [25] use a flux coupling-type SFCL to reduce successive commutation failures of the HVdc system. However, since the SFCLs operate based on a quenching characteristic, they are not controllable and have not the ability to suppress the fault current proportional to the reduced extinction angle. In order to remedy this challenge, reference [26] develops a controllable commutation failure prevention module (CFPM), in which the fault current is suppressed to a desired value based on the fault intensity. Nevertheless, in the developed module, a large isolation transformer and an extra three-phase diode bridge are required which significantly increase its capital cost and power losses. In addition, the voltage drop caused by the inductor of the CFPM circuit under normal operating conditions enhances the probability of commutation failure.

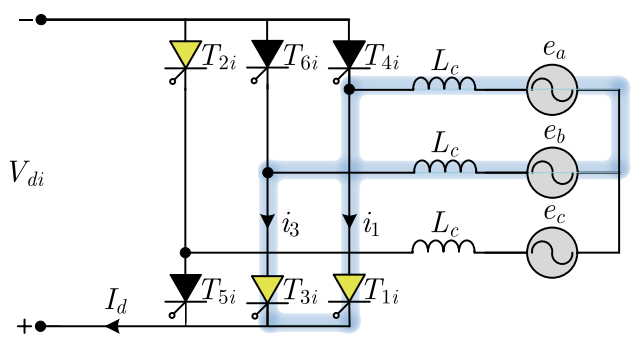

Fig. 1. Graetz bridge.

This article attempts to overcome the main challenges of the above-mentioned strategies through the development of a controllable commutation failure inhibitor (CCFI). Indeed, at no-fault conditions, the proposed CCFI acts similar to a CSCC, except that it does not cause excessive voltage drop on the inverter switches, because a significant portion of its capacitance is eliminated by a series inductor. Moreover, in spite of the fault current limiting based strategies, it is fully controllable and does not cause any voltage drop in the commutation circuit under normal conditions. In case a fault occurs at one of the receiving ac systems, its associated CCFI behaves like a fault current limiter to inhibit the occurrence of commutation failure at the inverter station.

The remainder of this article is organized as follows. Section II describes the commutation process and mechanism of commutation failure in line-commutated converters. In Section III, the structure of the proposed CCFI is presented and its operating principles are theoretically analyzed. In Section IV, the test network is introduced and the practical feasibility of the proposed CCFI is validated through laboratory testing. Finally, Section V concludes this article.

II. Commutation Process and Mechanism of Commutation Failure

Fig. 1 depicts the basic structure of a six-pulse converter at the inverter side which is referred to as Graetz bridge. The term six-pulse is due to the six commutations of switching operations per period, which forms a characteristic harmonic ripple of six times the fundamental frequency in the dc voltage. The Graetz bridge includes six thyristor valves, T_{1i} to T_{6i}, which are numbered according to the sequence they are triggered. At any instant, two valves are conducting, one from the upper group

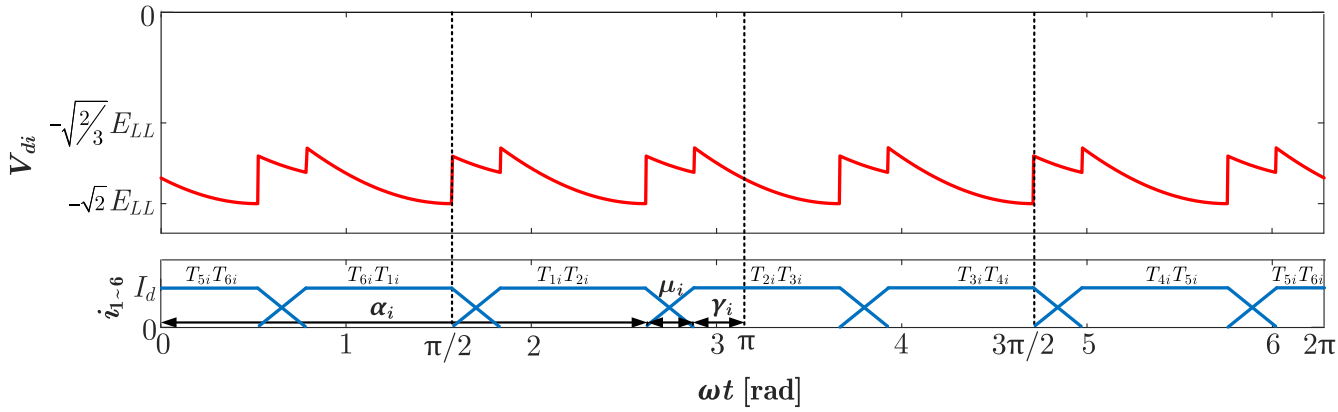

Fig. 2. Waveforms of the dc voltage and the currents through valves T_{1i} to T_{6i} for the inverter shown in Fig. 1.

of valves and second from the lower group. Fig. 2 displays the waveforms of the dc voltage and the currents through valves T_{1i} to T_{6i} for the inverter shown in Fig. 1. As can be seen from the figure, under steady-state conditions, each valve conducts for 120° and the interval between consecutive firing pulses is 60°. The instantaneous line-to-neutral voltages of each phase, $e_k(k = a, b, c)$, are expressed as

$$\begin{aligned} e_a &= \sqrt{2}E_{LL}\cos(\omega t + 60^\circ) \\ e_b &= \sqrt{2}E_{LL}\cos(\omega t - 60^\circ) \\ e_c &= \sqrt{2}E_{LL}\cos(\omega t - 180^\circ) \end{aligned} \tag{1}$$

where E_{LL} is the rms phase-to-phase ac voltage, and ω is the angular frequency in radians. The switching of current conduction from one of the thyristor valves to another in the same row of a converter bridge is referred to as commutation. The highlighted blue loop in Fig. 1 shows the electrical circuit for commutation from valve T_{1i} to valve T_{3i}. In this case, the firing angle, α_i, corresponds to the time when valve T_{3i} is fired after the commutation voltage $(e_b - e_a)$ has turned positive. Due to the inductance of the converter transformer and its connected ac system, the commutation process cannot be instantaneous and takes for a certain time, in which both valves T_{1i} and T_{3i} conduct. The angle corresponding to this time duration is termed as overlap angle, μ_i. After the overlap time, a reverse voltage requires to be applied across valve T_{1i} for a certain duration. This would remove the charges stored during its conduction process such that it can withstand a voltage in the forward direction. This negative voltage is applied during the time corresponding to the extinction angle, γ_i. The voltage equation during the commutation from valve T_{1i} to valve T_{3i} can be written as

$$e_b - e_a = \omega L_c \frac{\mathrm{d}i_3}{\mathrm{d}\omega t} - \omega L_c \frac{\mathrm{d}i_1}{\mathrm{d}\omega t} \tag{2}$$

where i_1 and i_3 are instantaneous currents flowing through valves T_{1i} and T_{3i}, respectively; L_c is the commutation reactance of each phase; and I_d is the dc current. Substituting (1) in (2), and using $i_1 = I_d - i_3$ gives

$$\sqrt{2}E_{LL}\sin(\omega t) = \omega L_c \frac{\mathrm{d}i_3}{\mathrm{d}\omega t} - \omega L_c \frac{\mathrm{d}(I_d - i_3)}{\mathrm{d}\omega t}. \tag{3}$$

Considering $\mathrm{d}I_d/\mathrm{d}\omega t = 0$, (3) becomes

$$\int_0^{I_d} 2\omega L_c \mathrm{d}i_3 = \int_{\alpha_i}^{\pi-\gamma_i} \sqrt{2}E_{LL}\sin(\omega t)\mathrm{d}\omega t \tag{4}$$

where α_i and γ_i are, respectively, firing angle and extinction angle of the thyristor valves at the inverter station. Therefore, I_d can be computed as

$$I_d = \frac{\sqrt{2}E_{LL}}{2\omega L_c}\left(\cos\alpha_i + \cos\gamma_i\right). \tag{5}$$

In case of a fault incident at the inverter ac side, the ac voltage magnitudes of the affected phases decrease which results in a dc voltage drop according to the principles of ac/dc conversion. Such a reduction in the dc voltage increases I_d in order to sustain the active power at the rated power of the inverter station. Accordingly, the overlap angle also increases which leads to a reduction in the extinction angle. When γ_i drops below the thyristor turn-OFF time, leads to the unexpected turn-ON of T_{1i} is supposed to be OFF, and a commutation failure takes place. In the next scheduled commutation, T_{4i} is also fired which creates a dc short circuit since both valves of a converter arm simultaneously conduct. This leads to a zero dc voltage across the faulty converter arm, and hence no active power can be transmitted through it [27]–[29].

III. Proposed CCFI

A. Structure and Operating Principles of the Proposed CCFI

Fig. 3 demonstrates the structure of the proposed CCFI in a hybrid ac/dc grid including one dc line and two receiving ac systems. As can be seen from the figure, it is composed of a thyristor-controlled inductor in series with a capacitor which operates as a double-function device by applying different firing angles to the thyristor valves. Under normal conditions, the CCFI behaves similar to a CSCC with a small capacitance which enhances the magnitude of the inverter commutating voltages and provides a larger commutation margin, while it does not cause excessive voltage stress on the inverter valves. In addition, it improves the system steady-state stability and reduces the transmission losses in the receiving ac systems. When a fault

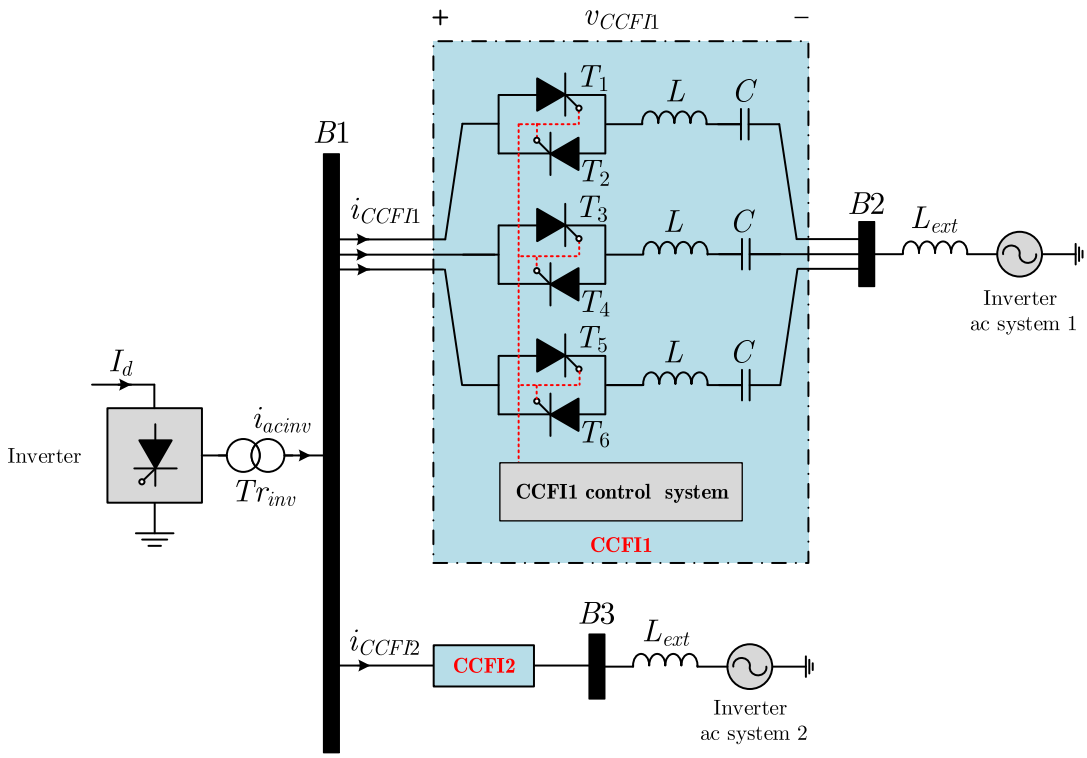

Fig. 3. Structure of the proposed CCFI in a hybrid ac/dc grid including one dc line and two receiving ac systems.

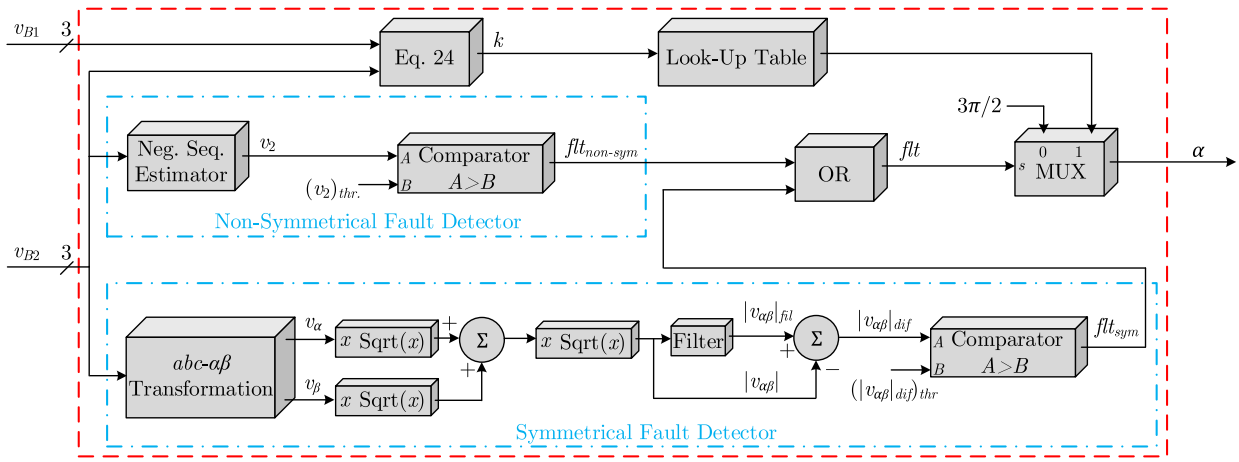

Fig. 4. Schematic diagram of CCFI1 control system.

occurs at one of the inverter ac systems, its corresponding CCFI limits the fault current depending on the reduced extinction angle. This would not only prevent the commutation failure in the inverter station, but also extend the lifespan of components in the inverter ac systems.

Fig. 4 depicts the schematic diagram of the CCFI1 control system shown in Fig. 3. According to the figure, fault occurrence at the inverter ac system 1 is recognized by either symmetrical or nonsymmetrical fault detector, depending on the fault type. In the nonsymmetrical fault detector, the negative-sequence voltage is used as fault detection criterion, since it is the only sequence which appears in all types of nonsymmetrical faults, i.e., single-line-to-ground, line-to-line, and line-to-line-to-ground faults. Once the measured negative-sequence voltage exceeded a predetermined threshold value, $(v_2)_{\text{thr}}$, signal $flt_{\text{non-Sym}}$ is issued and a nonsymmetrical fault is recognized.

However, for the detection of symmetrical faults, $abc{-}\alpha\beta$ transformation is applied. The idea of employing this transformation is that the magnitude of rotating vector $v_{\alpha\beta}$, $|v_{\alpha\beta}| = \sqrt{v_\alpha^2 + v_\beta^2}$, is a dc quantity for symmetrical three-phase voltages. In the developed CCFI, when a three-phase fault occurs,

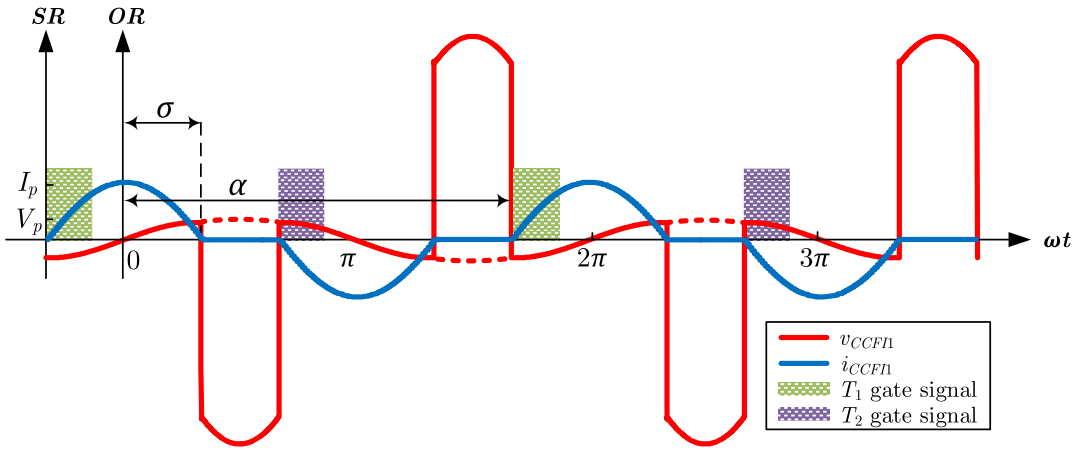

Fig. 5. Phase voltage and current waveforms of CCFI1.

$|v_{\alpha\beta}|$ is compared with its filtered signal, $|v_{\alpha\beta}|_{\text{fil}}$, which is considered as the prefault voltage. If $|v_{\alpha\beta}|_{\text{dif}} = |v_{\alpha\beta}|_{\text{fil}} - |v_{\alpha\beta}|$ is greater than a predefined threshold, then the symmetrical fault detector output is activated.

In case of a fault detection at inverter ac system 1, by either symmetrical or nonsymmetrical fault detector, CCFI1 is transferred to its fault current limiting mode through a multiplexer. Accordingly, a suitable firing angle is applied to CCFI1 valves depending on the reduced extinction angle to limit the fault current and inhibit the commutation failure.

B. CCFI Operation Analysis

Fig. 5 depicts the phase voltage and current waveforms of CCFI1 shown in Fig. 3 during steady-state conditions. In this figure, the time reference, termed as "original reference (OR)" is taken at the positive-going zero-crossing of v_{CCFI1}. However, for the simplicity of analysis, a shifted reference (SR) is considered which is taken when thyristor T_1 starts to conduct. Accordingly, v_{CCFI1} in terms of the shifted reference can be expressed as

$$\begin{aligned} v_{CCFI1,SR} &= V_p \sin(\omega t - \sigma) \\ &= V_p \sin(\omega t)\cos\sigma - V_p \cos(\omega t)\sin\sigma. \end{aligned} \tag{6}$$

The voltage equation across CCFI1 circuit can be written as

$$v_{CCFI1,SR} = v_{L,SR} + v_{C,SR}. \tag{7}$$

Substituting (6) in (7) and taking Laplace transform results in

$$\begin{aligned} &V_p \cos\sigma \left(\frac{\omega}{s^2+\omega^2}\right) - V_p \sin\sigma \left(\frac{s}{s^2+\omega^2}\right) \\ &= (LsI_{L,SR}(s) - Li_{L,SR}(0)) \\ &\quad + \left(\frac{1}{Cs} I_{C,SR}(s) + \frac{1}{s} v_{C,SR}(0)\right). \end{aligned} \tag{8}$$

Since L and C are connected in series, $I_{CCFI1,SR}(s) = I_{L,SR}(s) = I_{C,SR}(s)$. Also, $i_{L,SR}(0) = 0$ according to Fig. 5. Therefore, $I_{CCFI1,SR}(s)$ can be described as

$$\begin{aligned} I_{CCFI1,SR}(s) &= V_p \omega \cos\sigma L \frac{s}{(s^2+\omega^2)(s^2+\omega_0^2)} \\ &\quad - \frac{V_p \sin\sigma}{L} \frac{s^2}{(s^2+\omega^2)(s^2+\omega_0^2)} \\ &\quad - \frac{v_{C,SR}(0)}{L} \frac{1}{s^2+\omega_0^2} \end{aligned} \tag{9}$$

where $\omega_0 = \frac{1}{\sqrt{LC}}$ denotes the resonant angular frequency. Equation (9) can be expressed in the time domain by taking the Laplace inverse as

$$\begin{aligned} i_{CCFI1,SR} &= A\omega \cos\sigma(\cos\omega t - \cos\omega_0 t) \\ &\quad - A \sin\sigma(\omega_0 \sin\omega_0 t - \omega \sin\omega t) \\ &\quad - Dv_{C,SR}(0) \sin\omega_0 t \end{aligned} \tag{10}$$

where $A = \frac{V_p}{L(\omega_0^2 - \omega^2)}$ and $D = \frac{1}{L\omega_0}$. Simplifying (10) results in

$$\begin{aligned} i_{CCFI1,SR} &= A\omega \cos(\omega t - \sigma) - A\omega \cos\sigma \cos\omega_0 t \\ &\quad - (A\omega_0 \sin\sigma + Dv_{C,SR}(0)) \sin\omega_0 t. \end{aligned} \tag{11}$$

i_{CCFI1} in terms of the original time reference for the range of $[-\sigma, \sigma]$ can be obtained by adding σ/ω to the time variable in (11) which results in

$$\begin{aligned} i_{CCFI1} &= A\omega \cos\omega t - (A\omega \cos\sigma \cos\bar{\omega}\sigma \\ &\quad + A\omega_0 \sin\sigma \sin\bar{\omega}\sigma + Dv_{C,SR}(0) \sin\bar{\omega}\sigma) \cos\omega_0 t \\ &\quad + (A\omega \cos\sigma \sin\bar{\omega}\sigma - A\omega_0 \sin\sigma \cos\bar{\omega}\sigma \\ &\quad - Dv_{C,SR}(0) \cos\bar{\omega}\sigma) \sin\omega_0 t \end{aligned} \tag{12}$$

where $\bar{\omega} = \omega_0/\omega$. As can be seen from Fig. 5, in the steady-state conditions, i_{CCFI1} is an even function, and hence the coefficient of $\sin\omega_0 t$ in (12) takes a value of zero. Therefore, $v_{C,SR}(0)$ can be calculated by

$$v_{C,SR}(0) = \frac{A}{D}\omega \cos\sigma \frac{\sin\bar{\omega}\sigma}{\cos\bar{\omega}\sigma} - \frac{A}{D}\omega_0 \sin\sigma. \tag{13}$$

By substituting (13) into (12) and simplifying

$$i_{CCFI1} = A\omega\cos\omega t - \frac{A\omega\cos\sigma}{\cos\bar{\omega}\sigma}\cos\bar{\omega}\omega t. \tag{14}$$

As can be seen from Fig. 5, i_{CCFI1} has even and quarter-wave symmetry. Therefore, its Fourier series can be written as

$$i_{CCFI1} = \sum_n I_{CCFI1(n)}\cos n\omega t \tag{15}$$

where

$$I_{CCFI1(n)} = \begin{cases} 0 & \text{for } n \text{ even} \\ \frac{4}{\pi}\int_0^{\pi/2} i_{CCFI1}\cos n\omega t \mathrm{d}\omega t & \text{for } n \text{ odd.} \end{cases} \tag{16}$$

As a result, the rms value of the fundamental frequency component of i_{CCFI1} can be calculated by substituting (14) in (16)

$$I_{CCFI1(1),\text{rms}} = \frac{A\omega}{\pi\sqrt{2}}(2\sigma + \sin 2\sigma) - \frac{4A\omega}{\pi\sqrt{2}(\bar{\omega}^2-1)}(\bar{\omega}\cos^2\sigma\tan\bar{\omega}\sigma - \sin\sigma\cos\sigma). \tag{17}$$

Substituting $A = \frac{V_p}{L(\omega_0^2-\omega^2)} = \frac{CV_p\bar{\omega}^2}{\bar{\omega}^2-1}$ and $\sigma = 2\pi - \alpha$ in (17) results in

$$I_{CCFI1(1),\text{rms}} = \frac{V_{CCFI1,\text{rms}}C\omega\bar{\omega}^2}{(\bar{\omega}^2-1)}\left[\frac{2(2\pi-\alpha)}{\pi} + \frac{\sin 2(2\pi-\alpha)}{\pi} - \frac{4\bar{\omega}\cos^2(2\pi-\alpha)\tan\bar{\omega}(2\pi-\alpha)}{\pi(\bar{\omega}^2-1)} + \frac{4\sin(2\pi-\alpha)\cos(2\pi-\alpha)}{\pi(\bar{\omega}^2-1)}\right] \tag{18}$$

where $V_{CCFI1,\text{rms}} = V_p/\sqrt{2}$. The impedance magnitude of the LC circuit in CCFI1 can be determined as

$$|Z_{LC}| = \frac{1}{\omega C} - \omega L = \frac{1-\frac{\omega^2}{\omega_0^2}}{\omega C} = \frac{\bar{\omega}^2-1}{C\omega\bar{\omega}^2}. \tag{19}$$

Substituting (19) in (18) results in

$$I_{CCFI1(1),\text{rms}} = \frac{kV_{CCFI1,\text{rms}}}{|Z_{LC}|} \tag{20}$$

where k is the term inside the square bracket of (18). For any given thyristor firing angle, α, the fundamental frequency component of CCFI1 impedance magnitude can be obtained using (20) as follows:

$$Z_{CCFI1(1)} = \frac{V_{CCFI1,\text{rms}}}{I_{CCFI1(1),\text{rms}}} = \frac{|Z_{LC}|}{k}. \tag{21}$$

Fig. 6 shows the relationship between parameter k and CCFI1 thyristor firing angle considering $\bar{\omega} = 3$, at which symmetry of the current waveform is preserved and the thyristor arms are equally stressed. Under normal conditions, the thyristor firing angle is $3\pi/2$, and k takes the value of 1. Accordingly, $Z_{CCFI1(1)}$ becomes equivalent to the LC circuit impedance magnitude, $|Z_{LC}|$. Hence, by considering $X_C > X_L$, the power system stability and power transfer capability can be improved

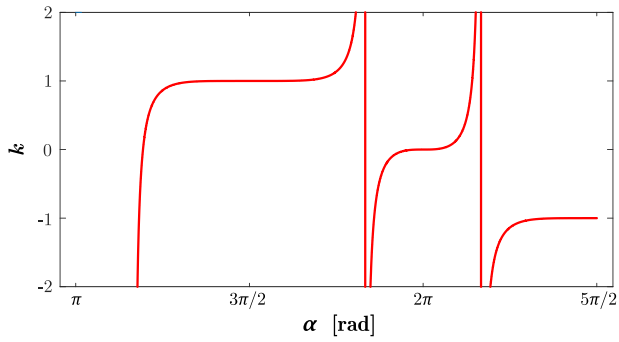

Fig. 6. Relationship between parameter k and CCFI1 thyristor firing angle.

at no-fault conditions. In case of a fault incident, the CCFI1 thyristor firing angle is selected in the range of $6.28 < \alpha < 6.72$ rad depending on the reduced extinction angle, to limit $I_{CCFI1(1),\text{rms}}$ and inhibit the commutation failures. It shall be noted that the insertion of any type of fault current limiter (FCL) decreases the magnitude of short-circuit current and may lead to the maloperation of protective relays, since it affects the admittance matrix of the network. However, it is a common practice that the influenced relays are readjusted and recoordinated with each other after the installation of an FCL based on the maximum limited current by the FCL. As a result, readjustment of the relays located on each inverter ac system after implementation of the proposed strategy would be necessary.

Neglecting the commutation overlap for the inverter shown in Fig. 3, the rms value of the fundamental frequency component of inverter ac current can be calculated using Fourier analysis as

$$I_{\text{inv}(1),\text{rms}} = \frac{1}{\pi\sqrt{2}}\int_{-\pi}^{\pi} I_d\cos\omega t \mathrm{d}\omega t = \frac{\sqrt{6}}{\pi}I_d. \tag{22}$$

By substituting (5) in (22) and considering $I_{CCFI1(1),\text{rms}} = mI_{\text{inv}(1),\text{rms}}$, where m is a constant between 0 and 1, $I_{CCFI1(1),\text{rms}}$ can be written as

$$I_{CCFI1(1),\text{rms}} = \frac{m\sqrt{3}E_{LL}}{\pi\omega L_c}\left(\cos\alpha_i + \cos\gamma_i\right). \tag{23}$$

By equating (18) and (23), and considering a minimum commutation margin, $\gamma_{\min}$, parameter k is obtained as

$$k = \frac{m\sqrt{3}E_{LL}(\bar{\omega}^2-1)(\cos\alpha_i + \cos\gamma_{\min})}{\pi L_c C\omega^2\bar{\omega}^2 V_{CCFI1,\text{rms}}}. \tag{24}$$

As discussed before, under normal conditions, CCFI1 is used to compensate for the inductive reactance of its corresponding ac line. The resonant angular frequency of the compensated ac line by CCFI1 is expressed as

$$\omega_{0,\text{tot}} = \omega\underbrace{\sqrt{k_{\text{ser}}}}_{\bar{\omega}_{\text{tot}}} = \omega\sqrt{\frac{X_C}{X_{L_{\text{ext}}}+X_L}} = \frac{1}{\sqrt{C(L_{\text{ext}}+L)}} \tag{25}$$

where k_{ser} is the compensation degree of the compensated ac line which is typically in the range of 25%–70% [30]; L and C are CCFI1 parameters; and L_{ext} is the equivalent series inductance connected to CCFI1. It shall be noted that even though the practical upper limit of k_{ser} is 70%, in the proposed strategy, in order to prevent the excessive voltage stress on the inverter

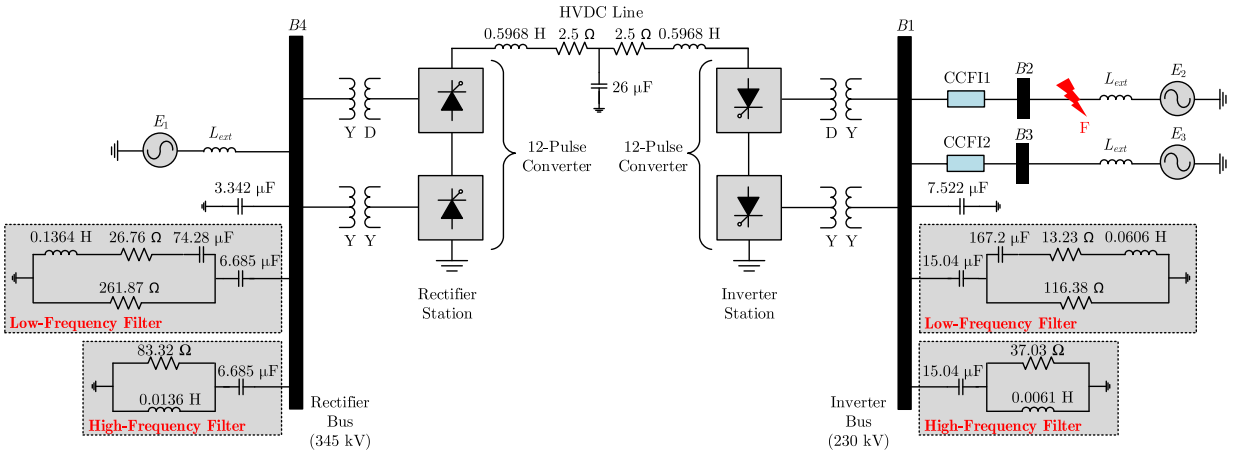

Fig. 7. Single-line diagram of the test network.

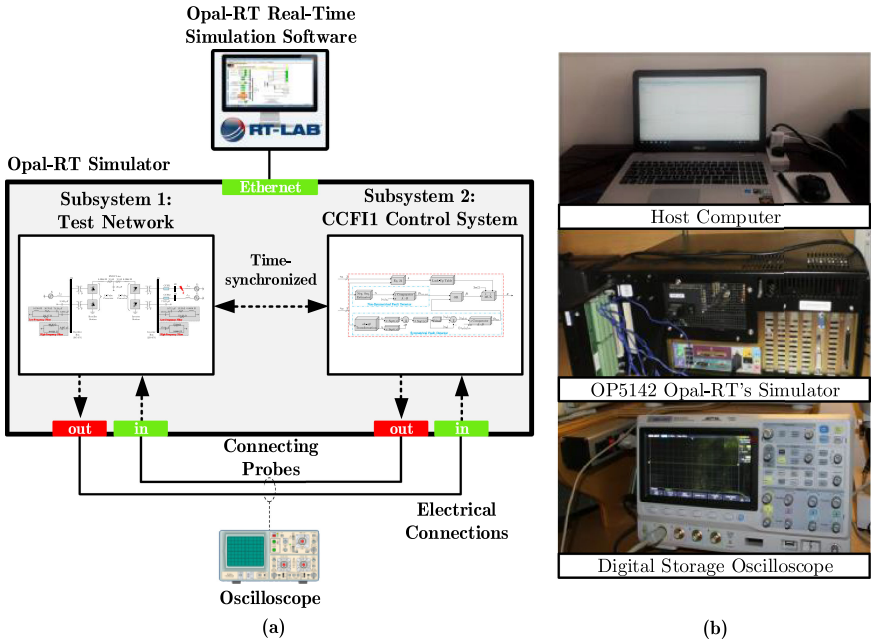

Fig. 8. Schematic diagram of the experimental test. (a) Experimental setup. (b) Experimental arrangement.

valves, only 30% of the ac line is compensated. The resonant angular frequency of CCFI1 is $\omega_0 = \omega\bar{\omega} = 1/\sqrt{LC}$. Therefore

$$C = \frac{1}{L\bar{\omega}^2\omega^2}. \tag{26}$$

By substituting (26) in (25), L is determined as

$$L = \frac{k_{\text{ser}}L_{\text{ext}}}{\bar{\omega}^2 - k_{\text{ser}}}. \tag{27}$$

The capacitance of CCFI1 is also determined by substituting (27) in (26)

$$C = \frac{\bar{\omega}^2 - k_{\text{ser}}}{k_{\text{ser}}\omega^2\bar{\omega}^2 L_{\text{ext}}}. \tag{28}$$

In order to better illustrate the selection of parameters in the proposed CCFI, let's assume $L_{\text{ext}} = 16$ mH, $\bar{\omega} = 3$, and the frequency of the inverter ac system is 50 Hz. In this case, if the series compensation degree of 25% is desired, then a 0.45 mH inductor (corresponding to inductive reactance of 0.14 Ω) and a 2462.66-μF capacitor (corresponding to capacitive reactance of 1.29 Ω) are required according to (27) and (28), respectively. While for $k_{\text{ser}} = 70\%$, the suitable CCFI parameters are $L = 1.34$ mH (corresponding to inductive reactance of 0.42 Ω) and $C = 834.29\,\mu$F (corresponding to capacitive reactance of 3.81 Ω). As a result, the size and cost-effectiveness of the proposed CCFI depend on the degree of series compensation. In fact, the larger the degree of series compensation, the greater inductive and capacitive reactance required. However, the optimal

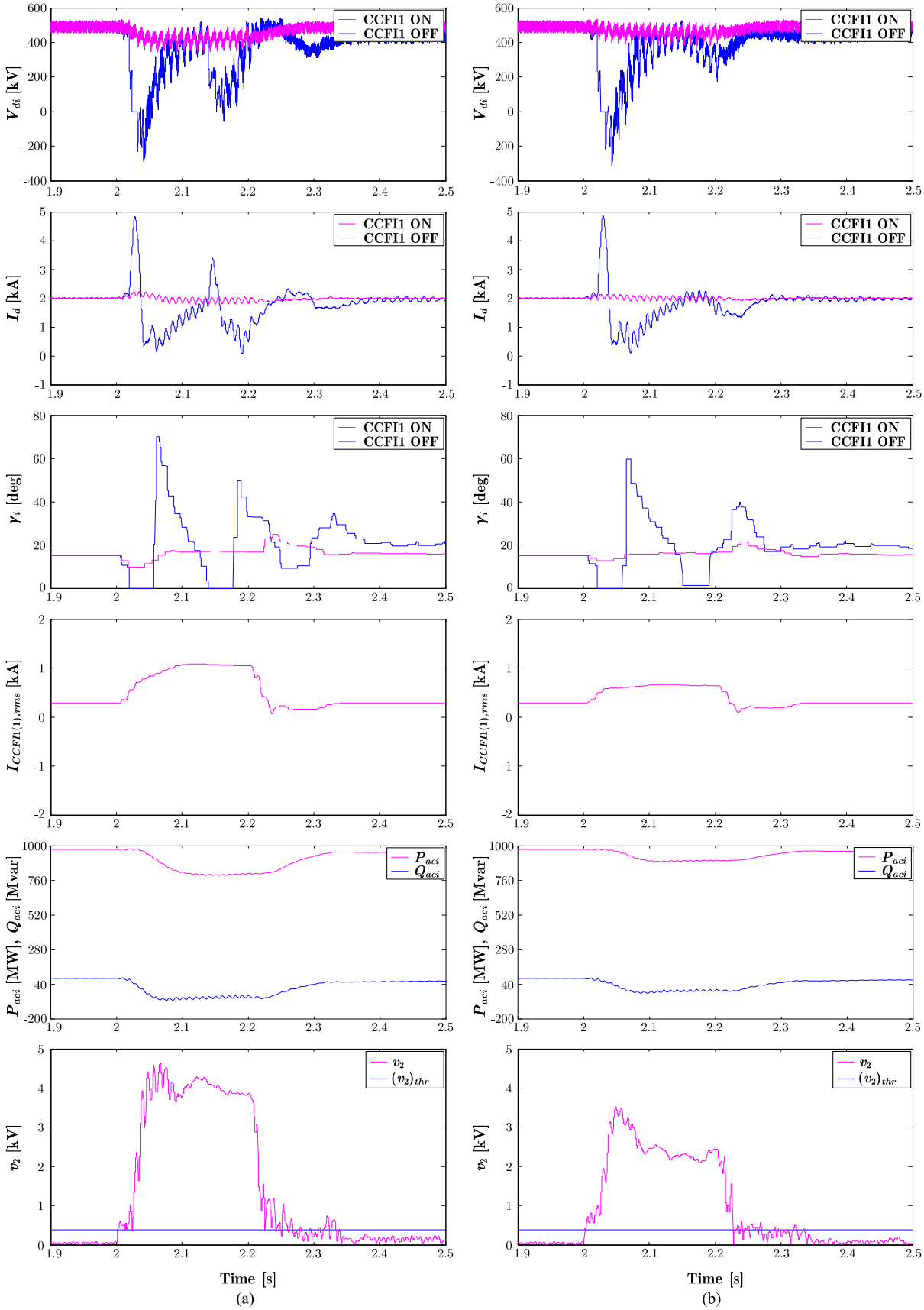

Fig. 9. The results obtained from the experimental test of the proposed CCFI under different fault types. (a) Single-line-to-ground fault. (b) Double-line fault. (c) Double-line-to-ground fault. (d) Three-phase fault.

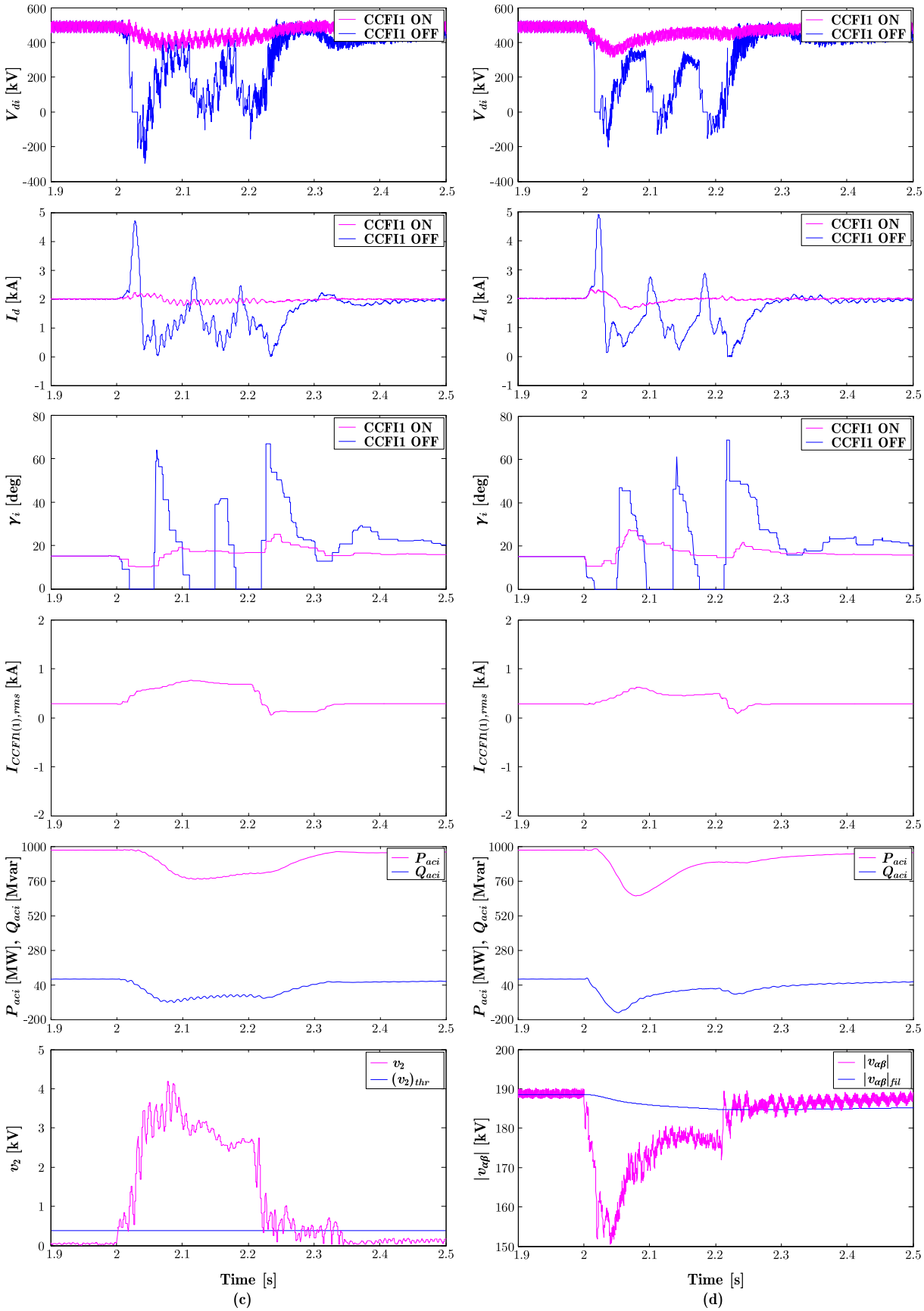

Fig. 9. (Continued) The results obtained from the experimental test of the proposed CCFI under different fault types. (a) Single-line-to-ground fault. (b) Double-line fault. (c) Double-line-to-ground fault. (d) Three-phase fault.

value of k_{ser} should be determined based on the voltage stress on the converter valves, and the stability and power transfer capability of the inverter ac system.

IV. Experimental Validation

Fig. 7 shows the single-line diagram of the test network which connects the ac system in the rectifier side to two identical ac systems in the inverter side through a monopolar 500 kV and 1000 MW HVdc system. The HVdc system consists of a dc line modeled by a T circuit, two 12-pulse converters, ac filters, and shunt capacitors in both rectifier and inverter sides. In order to verify the effectiveness of the proposed CCFI under real-time conditions, an experimental setup has been developed. The Opal-RT Simulator is one of the most advanced real-time simulation devices which enables users to conduct high-fidelity simulations and test even the most complex systems with ease and at the lowest possible cost. Fig. 8 demonstrates the schematic diagram of the experimental test. As shown in the figure, first, the MATLAB/Simulink models are built in a host computer installed with Opal RT-Lab software. The host computer is linked to the Opal-RT simulator through ethernet, and then the simulation results are observed in a digital storage oscilloscope via connecting probes. The entire real-time model consists of two separate subsystems, where subsystem 1 denotes the test network, and subsystem 2 represents the control system of CCFI1. The input signals of subsystem 2 which are produced by subsystem 1 include the three-phase voltages across CCFI1. Also, the output of subsystem 2, i.e., CCFI1 thyristor firing angle, forms the input of subsystem 1.

The results obtained from the experimental test of the proposed CCFI under different fault types, i.e., single-line-to-ground, double-line, double-line-to-ground, and three-phase faults, are displayed in Fig. 9. In all analyzed cases, fault F (as indicated in Fig. 7) is applied at $t = 2$ s for a duration of 0.2 s. In this figure, V_{di} and I_d, respectively, denote the measured voltage and current of the HVdc line at the inverter station; γ_i represents the inverter extinction angle; $I_{CCFI1(1),\text{rms}}$ is the rms value of the fundamental frequency component of current flowing through CCFI1; P_{aci} and Q_{aci} are, respectively, active and relative powers measured at the inverter bus; also, v_2 and $|v_{\alpha\beta}|$ represent the negative-sequence voltage and the magnitude of rotating vector $v_{\alpha\beta}$, respectively.

As can be seen in all cases, before the fault occurrence, the inverter extinction angle has a constant value which is controlled by the HVdc control system. Also, $I_d = 2$ kA and $V_{di} = 500$ kV which leads to the transmission of 1000 MW active power through the HVdc line. Under such conditions, CCFI1 thyristor firing angle takes the value of $3\pi/2$, and hence, CCFI1 operates as a capacitor which improves the steady-state stability of its connected line.

With reference to Fig. 9(a), when a single-line-to-ground fault happens, the inverter ac voltage, and thus, the involved commutating voltages are reduced in magnitude. Such a voltage drop reduces the dc voltage, V_{di}, which leads to an increase in the dc current. Since the overlap angle is proportional to the dc current, it also increases and reduces the extinction angle, leading to two consecutive commutation failures initiated at $t = 2.02$ s.

In order to inhibit the successive commutation failures, CCFI1 control system is activated once the fault is detected by the nonsymmetrical fault detector. As can be seen from Fig. 9, both harmonics and the delay associated with the negative-sequence voltage phasor measurement have influenced the voltage waveforms. In order to eliminate such challenges, the threshold values are selected such that the fault detection signal is triggered up to a maximum of 2 ms after the fault initiation time and the harmonic distortion does not lead to the deactivation of the CCFI1 during the fault. Subsequently, the value of k is determined using (24) such that the minimum commutation margin is ensured ($k = 0.22$ in this case). Finally, the corresponding value of CCFI1 thyristor firing angle, $\alpha = 6.622$ rad, is selected using a lookup table which has been set according to Fig. 6. This leads to the limitation of the fault current up to 14.11 kA, thereby commutation failure is prevented at the inverter station. A similar analysis can be performed for other types of faults, except that $|V_{\alpha\beta}|_{\text{dif}}$ is used as a fault detection signal for the symmetrical three-phase fault.

V. Conclusion

In this article, a CCFI has been proposed which consists of a thyristor-controlled inductor in series with a capacitor. The developed CCFI operates as a double-function device by applying different firing angles to its thyristor switches. At no-fault conditions, the CCFI improves the steady-state stability and power transfer capability of the inverter ac lines due to the presence of the series capacitance. In case of a fault incident at one of the inverter ac systems, its corresponding CCFI switches to the fault current limiting mode and inhibits the commutation failure. The salient feature of the developed CCFI is that it is fully controllable and has a noncomplex structure and control circuit. Besides, it neither causes excessive voltage stress on the inverter switches nor any voltage drop on the commutation circuit. To verify the effectiveness of the proposed strategy under real-time conditions, several fault cases were experimentally tested. The results showed that the developed CCFI can effectively prevent successive commutation failures at the inverter station.

References

[1] G. Li *et al.*, "Feasibility and reliability analysis of LCC DC Grids and LCC/VSC hybrid dc grids," *IEEE Access*, vol. 7, pp. 22445–22456, 2019.
[2] Y. Xue, X. Zhang, and C. Yang, "Series capacitor compensated ac filterless flexible LCC HVDC with enhanced power transfer under unbalanced faults," *IEEE Trans. Power Syst.*, vol. 34, no. 4, pp. 3069–3080, Jul. 2019.
[3] X. Li, C. Liu, and Y. Lou, "Start-up and recovery method with LCC–HVDC systems participation during ac/dc system black-starts," *IET Gener. Transmiss. Distrib.*, vol. 14, no. 3, pp. 362–367, 2020.
[4] J. Chen, Q. Wang, and X. Zhu, "Evaluation of commutation failure risk for HVDC caused by harmonic voltage," in *Proc. IEEE 3rd Conf. Energy Internet Energy Syst. Integration (EI2)*, 2019, pp. 248–252.
[5] Z. Wei, Y. Yuan, X. Lei, H. Wang, G. Sun, and Y. Sun, "Direct-current predictive control strategy for inhibiting commutation failure in HVDC converter," *IEEE Trans. Power Syst.*, vol. 29, no. 5, pp. 2409–2417, Sep. 2014.
[6] S. Tamai, H. Naitoh, F. Ishiguro, M. Sato, K. Yamaji, and N. Honjo, "Fast and predictive HVDC extinction angle control," *IEEE Trans. Power Syst.*, vol. 12, no. 3, pp. 1268–1275, Aug. 1997.

[7] C. V. Thio, J. B. Davies, and K. L. Kent, "Commutation failures in HVDC transmission systems," *IEEE Trans. Power Del.*, vol. 11, no. 2, pp. 946–957, Apr. 1996.

[8] S. Mirsaeidi and X. Dong, "An enhanced strategy to inhibit commutation failure in line-commutated converters," *IEEE Trans. Ind. Electron.*, vol. 67, no. 1, pp. 340–349, Jan. 2020.

[9] C. Guo, Y. Liu, C. Zhao, X. Wei, and W. Xu, "Power component fault detection method and improved current order limiter control for commutation failure mitigation in HVDC," *IEEE Trans. Power Del.*, vol. 30, no. 3, pp. 1585–1593, Jun. 2015.

[10] J. Bauman and M. Kazerani, "Commutation failure reduction in HVDC systems using adaptive fuzzy logic controller," *IEEE Trans. Power Syst.*, vol. 22, no. 4, pp. 1995–2002, Nov. 2007.

[11] Y. Z. Sun, L. Peng, F. Ma, G. J. Li, and P. F. Lv, "Design a fuzzy controller to minimize the effect of HVDC commutation failure on power system," *IEEE Trans. Power Syst.*, vol. 23, no. 1, pp. 100–107, Feb. 2008.

[12] A. Hansen and H. Havemann, "Decreasing the commutation failure frequency in HVDC transmission systems," *IEEE Trans. Power Del.*, vol. 15, no. 3, pp. 1022–1026, Jul. 2000.

[13] S. Mirsaeidi, X. Dong, D. Tzelepis, D. M. Said, A. Dyko, and C. Booth, "A predictive control strategy for mitigation of commutation failure in LCC-based HVDC systems," *IEEE Trans. Power Electron.*, vol. 34, no. 1, pp. 160–172, Jan. 2019.

[14] W. Yao, C. Liu, J. Fang, X. Ai, J. Wen, and S. Cheng, "Probabilistic analysis of commutation failure in LCC-HVDC system considering the CFPREV and the initial fault voltage angle," *IEEE Trans. Power Del.*, pp. 1–1, 2019.

[15] Y. Xue, X. P. Zhang, and C. Yang, "Elimination of commutation failures of LCC HVDC system with controllable capacitors," *IEEE Trans. Power Syst.*, vol. 31, no. 4, pp. 3289–3299, Jul. 2016.

[16] R. Bunch and D. Kosterev, "Design and implementation of ac voltage dependent current order limiter at Pacific HVDC Intertie," *IEEE Trans. Power Del.*, vol. 15, no. 1, pp. 293–299, Jan. 2000.

[17] C. W. Taylor and S. Lefebvre, "HVDC controls for system dynamic performance," *IEEE Trans. Power Syst.*, vol. 6, no. 2, pp. 743–752, May 1991.

[18] M. Jafar and M. Molinas, "Effects and mitigation of post-fault commutation failures in line-commutated HVDC transmission system," in *Proc. 2009 IEEE Int. Symp. Ind. Electron.*, Seoul, South Korea, Jul. 2009, pp. 81–85.

[19] F. Karlecik-Maier, "A new closed loop control method for HVDC transmission," *IEEE Trans. Power Del.*, vol. 11, no. 4, pp. 1955–1960, Oct. 1996.

[20] M. O. Faruque, Y. Zhang, and V. Dinavahi, "Detailed modeling of CIGRE HVDC Benchmark system using PSCAD/EMTDC and PSB/SIMULINK," *IEEE Trans. Power Del.*, vol. 21, no. 1, pp. 378–387, Jan. 2006.

[21] H. I. Son and H. M. Kim, "An algorithm for effective mitigation of commutation failure in high-voltage direct-current systems," *IEEE Trans. Power Del.*, vol. 31, no. 4, pp. 1437–1446, Aug. 2016.

[22] T. Gao and X. Ma, "Comparison of CCC and LCC in HVDC system," *Energy Procedia*, vol. 16, no. 1, pp. 842–848, Jan. 2012.

[23] D. Jovcic, "Thyristor-based HVDC with forced commutation," *IEEE Trans. Power Del.*, vol. 22, no. 1, pp. 557–564, Jan. 2007.

[24] H. Lee, G. T. Son, J. Yoo, and J. Park, "Effect of a SFCL on commutation failure in a HVDC system," *IEEE Trans. Appl. Supercond.*, vol. 23, no. 3, pp. 5 600 104–5 600 104, Jun. 2013.

[25] L. Chen, H. Pan, C. Deng, F. Zheng, Z. Li, and F. Guo, "Study on the application of a flux-coupling-type superconducting fault current limiter for decreasing HVDC commutation failure," *Can. J. Elect. Comput. Eng.*, vol. 38, no. 1, pp. 10–19, 2015.

[26] S. Mirsaeidi, X. Dong, and D. M. Said, "A fault current limiting approach for commutation failure prevention in LCC-HVDC transmission systems," *IEEE Trans. Power Del.*, vol. 34, no. 5, pp. 2018–2027, Oct. 2019.

[27] J. Liu, Q. Liu, R. Jiang, L. Zhang, and R. Wang, "Analysis of commutation failure of HVDC transmission system with wind farm," in *2018 2nd IEEE Conf. Energy Internet Energy Syst. Integration (EI2)*, 2018, pp. 1–6.

[28] Z. Ren, J. Li, J. He, Y. Sun, and Y. Liu, "Study on fault current suppression and commutation failure in inverter side of 1100 kV DC system," in *Proc IEEE Int. Conf. High Voltage Eng. Appl.*, 2018, pp. 1–4.

[29] Y. Lu, H. Zhang, Y. Cao, C. Ma, D. Yang, and H. Ma, "A control strategy for suppressing HVDC continuous commutation failure risk under weak AC state," in *Proc. IEEE 3rd Int. Conf. Green Energy and Appl.*, 2019, pp. 35–39.

[30] E. M. J, *Reactive Power Control in Electric Systems*. New York, NY, USA: Wiley, 1982.

Sohrab Mirsaeidi (Member, IEEE) received the Ph.D. degree in electrical engineering from the Universiti Teknologi Malaysia (UTM), Johor Bahru, Malaysia, in 2016.

From 2016 to 2019, he furthered his postdoctoral fellowship at the Department of Electrical Engineering, Tsinghua University, Beijing China.

Currently, he is an Associate Professor with the School of Electrical Engineering, Beijing Jiaotong University, Beijing, China. He has authored or coauthored more than 50 papers and two books in the field of microgrids and large-scale power systems. His main research interests include control and protection of large-scale hybrid ac/dc grids and microgrids, power system stability, and application of power electronics in power systems.

Dr. Mirsaeidi is a member of IET, CIGRE, and Chinese Society of Electrical Engineering (CSEE).

Dimitrios Tzelepis (Member, IEEE) received the B.Eng.(hons.) degree in electrical engineering from the Technological Education Institution of Athens, Athens, Greece, in 2013, and the M.Sc. degree in wind energy systems and the Ph.D. degree from the University of Strathclyde, Glasgow, U.K., in 2014 and 2017, respectively.

He is currently a Postdoctoral Researcher with the Department of Electronic and Electrical Engineering, University of Strathclyde. His research interests include the area of power system protection, automation, and control of future electricity grids, incorporating increased penetration of renewable energy sources and high voltage direct current interconnections. His main research methods include implementation of intelligent algorithms for protection, fault location, and control applications including the utilization of machine learning methods and advanced and intelligent signal processing techniques. He is also interested in the application, control, and protection of hybrid ac/dc grids including super-conducting feeders, nonhomogeneous transmission lines, and advanced sensing technologies. Additionally, he is investigating potential solutions toward the optimized performance of active distribution networks both in off-grid and on-grid modes to facilitate a wide suite of grid services and control capabilities.

Jinghan He (Fellow, IEEE) received the M.Sc. degree from Tianjin University, Tianjin, China, in 1994, and the Ph.D. degree from Beijing Jiaotong University, Beijing, China, in 2007, all in electrical engineering.

She is currently a Professor and Dean with the School of Electrical Engineering, Beijing Jiaotong University. Her main research interests include power system protection, HVdc systems, and applications of intelligent system techniques to power system monitoring, protection, and control.

Xinzhou Dong (Fellow, IEEE) was born in Shaanxi, China, in 1963. He received the B.Sc., M.Sc., and Ph.D. degrees in electrical engineering from Xi'an Jiaotong University, Shaanxi, China, in 1983, 1991, and 1996, respectively.

From 1997 to 1998, he furthered his postdoctoral research with the Electrical Engineering Station, Tianjin University, Tianjin, China. Since 1999, he has been with Tsinghua University, Beijing, China, where he is currently a Professor with the Department of Electrical Engineering, and Director of the International Union Research Center of Beijing on Green Energy and Power Safety. His research interests include protective relaying, fault location, and the application of wavelet transforms in power systems. He has authored or coauthored more than 200 journal papers.

Dr. Dong is a fellow of IET.

Dalila Mat Said (Senior Member, IEEE) received the B.Eng. and M.Eng. degrees in electrical engineering, and the Ph.D. degree in power quality from the Universiti Teknologi Malaysia (UTM), Malaysia, in 2000, 2002, and 2012, respectively.

Currently, she is an Associate Professor and Deputy Director at the Centre of Electrical Energy Systems, Faculty of Electrical Engineering, Universiti Teknologi Malaysia (UTM). She has 15 years of experience in teaching electrical engineering courses and supervision of more than 30 undergraduate, and 26 postgraduate students. She has an experience within the area of power quality consultancy. From 2010 to 2014, she was involved in the Power Quality Baseline Study in a Peninsular Malaysia under the Energy Commission of Malaysia.

Prof. Said is a Registered Member with the Board of Engineer (BEM), Graduate Member of the Institute of Engineers (IEM), and member of IET. Her research interests include power quality and power system measurement and monitoring.

Campbell Booth received the B.Eng. and Ph.D. degrees in electrical and electronic engineering from the University of Strathclyde, Glasgow, U.K., in 1991 and 1996, respectively.

He is currently a Professor and the Head of Department for Electronic and Electrical Engineering, University of Strathclyde. His research interests include power system protection, plant condition monitoring and intelligent asset management, applications of intelligent system techniques to power system monitoring, protection, and control, knowledge management, and decision.